

Angle-resolved photoemission spectroscopy of electron-doped cuprate superconductors: Isotropic electron-phonon coupling

Seung Ryong Park¹, D. J. Song¹, C. S. Leem¹, Chul Kim¹, C. Kim^{1,*}, B. J. Kim², and H. Eisaki³

¹*Institute of Physics and Applied Physics, Yonsei University, Seoul, Korea*

²*School of Physics and Center for Strongly Correlated Materials Research, Seoul National University, Seoul, Korea and*

³*AIST Tsukuba Central 2, Umezono, Tsukuba, Ibaraki, 305-8568, Japan*

(Dated: October 27, 2018)

We have performed high resolution angle resolved photoemission (ARPES) studies on electron doped cuprate superconductors $\text{Sm}_{2-x}\text{Ce}_x\text{CuO}_4$ ($x=0.10, 0.15, 0.18$), $\text{Nd}_{2-x}\text{Ce}_x\text{CuO}_4$ ($x=0.15$) and $\text{Eu}_{2-x}\text{Ce}_x\text{CuO}_4$ ($x=0.15$). Imaginary parts of the electron removal self energy show step-like features due to an electron-bosonic mode coupling. The step-like feature is seen along both nodal and anti-nodal directions but at energies of 50 and 70 meV, respectively, independent of the doping and rare earth element. Such energy scales can be understood as being due to preferential coupling to half- and full-breathing mode phonons, revealing the phononic origin of the kink structures. Estimated electron-phonon coupling constant λ from the self energy is roughly independent of the doping and momentum. The isotropic nature of λ is discussed in comparison with the hole doped case where a strong anisotropy exists.

PACS numbers: 74.25.Jb, 74.72.-h, 79.60.-i

Electron-bosonic mode coupling in solids manifests itself as a slope change in the dispersion or a “kink” in angle resolved photoemission (ARPES) dispersions.¹ ARPES studies have been extensively performed to obtain information on the electron-bosonic mode coupling (EBC)^{2,3,4,5,6,7} in high temperature superconductors (HTSCs) to find out what mediates the electron pairing. In spite of the extensive studies, controversy still exists on what causes the strong kink structure in ARPES spectra. The controversy can be rooted in the fact that there exists two bosonic modes with similar energy scales in hole doped HTSCs that may couple to quasi-particles, i.e., phonons and magnetic resonance modes. Optical phonons have energies between 40 and 90 meV^{8,9} while the magnetic resonance mode from neutron experiments shows an energy scale of 40 meV^{10,11}. Various devised ARPES experiments have been performed to pin point which mode causes the kink effects. However, the controversy will continue because the two energy scales are similar.

The magnetic mode in electron doped HTSCs meanwhile has been discovered only recently^{12,13}. While the energy scales of the optical phonons in the CuO_2 planes are similar between electron and hole doped cuprates, the magnetic mode in electron doped cuprates is found to be much smaller (~ 10 meV or smaller). Therefore, it should be easier to discern the two effects in electron doped HTSCs. In addition, recent progress in the crystal growth technique provides high quality samples suitable for EBC studies¹⁴. This recent progress gives us an important opportunity to study the kink effects in electron doped HTSCs. In fact, there is a recent report on this issue from the scanning tunnelling spectroscopy¹⁵. Motivated by this issue, we performed ARPES experiments on various electron doped systems of $\text{Sm}_{2-x}\text{Ce}_x\text{CuO}_4$ (SCCO), $\text{Nd}_{2-x}\text{Ce}_x\text{CuO}_4$ (NCCO) and $\text{Eu}_{2-x}\text{Ce}_x\text{CuO}_4$ (ECCO) with specific aim on the EBC studies. Our re-

sults show a clear evidence for electron-phonon coupling (EPC). Surprisingly, the coupling is isotropic in a strong contrast to the hole doped case. This fact should help to advance our comprehensive understanding of HTSCs over the entire phase diagram.

SCCO ($x=0.10, 0.15$ and 0.18), NCCO ($x=0.15$) and ECCO ($x=0.15$) single crystals were grown by the travelling-solvent floating-zone method. Relative Ce concentration was determined by Ce core-level photoemission and found to be consistent with the nominal values. NCCO, SCCO and ECCO were reduced by annealing in N_2 for 10 hours at 960, 900, 850 C, respectively, and then in oxygen for 20 hours at 500 C to induce superconductivity. T_c was determined to be 0, 17, 9, 23 and 0 K by magnetic susceptibility measurements for SCCO($x=0.10$), SCCO($x=0.15$), SCCO($x=0.18$), NCCO and ECCO samples, respectively. ARPES experiments were performed at beamline 5-4 of the Stanford Synchrotron Radiation Laboratory using 16.5 eV photons with an energy resolution of 14 meV. Samples were cleaved *in situ* and laser aligned. The chamber pressure was better than 4×10^{-11} torr and the temperature was kept at 15 K.

Fig. 1 (a)-(d) shows ARPES data along the nodal direction from the SCCO samples with $x=0.15$ and 0.18 . $x=0.1$ data is not shown because the feature is too broad to discuss the EBC. The raw data and the momentum distribution curve (MDC) dispersions show kink-like features at around 50 meV (marked by the arrows), strongly suggesting an EBC at that energy. However, it was shown that electronic structures of electron doped HTSCs show band folding effects due to possible $\sqrt{2} \times \sqrt{2}$ ordering^{17,20}. In fact, $x=0.15$ data has a nodal gap, as shown in the inset of Fig. 1 (b), stemming from a band folding effect¹⁴. In such case, it is difficult to judge if the bend in the dispersion is a kink or from band folding effects, especially for the nodal region.

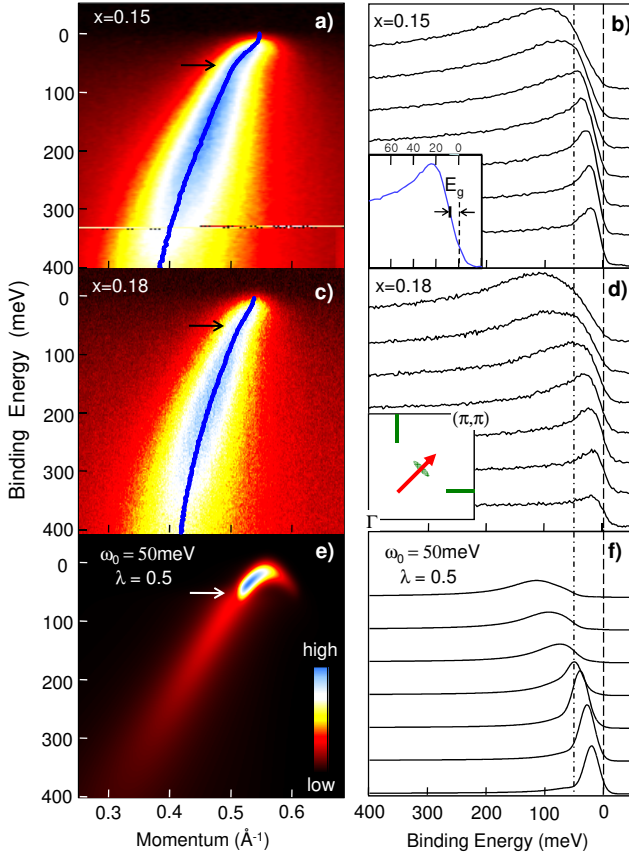


FIG. 1: (Color online) Intensity maps of ARPES data along the nodal direction from (a) $x=0.15$ and (c) 0.18 samples of SCCO. The lines in panels are the MDC dispersions while the arrows mark the energy where the kink structure appears in the dispersion. Panels (b) and (d) plot the EDC stacks of the data near the top of the band. The vertical dash-dot line marks the kink energy. The inset in panel (b) shows the lowest binding energy feature which remains below the Fermi level. The inset in panel (d) depicts the direction of the cuts in the Brillouin zone. Simulation results on EBC for a folded bare band is shown in panel (e) with EDCs in panel (f) in a similar fashion to the experimental data.

To see if one could still observe a kink structure in spite of a band folding effect, we plot in Fig. 1 (e) a simulated ARPES spectral function $A(k, \omega)$ of a folded band with a 50 meV Einstein phonon. The bare band was taken from the published nodal dispersion of SCCO¹⁴ and a moderate EPC constant $\lambda = 0.5$ was used. One finds that the kink structure is still visible for a folded band with a moderate λ .

We will later provide discussions on the EBC based on the self energy analysis. However, one can already find some EBC aspects from the energy distribution curve (EDC) plots. Shown in Fig. 1 (f) are EDCs from the simulation data near the top of the band. Not only can one still see a kink-like dispersion, but also observe that the peak becomes considerably broad beyond the mode energy as scattering is allowed through EBC. Looking at

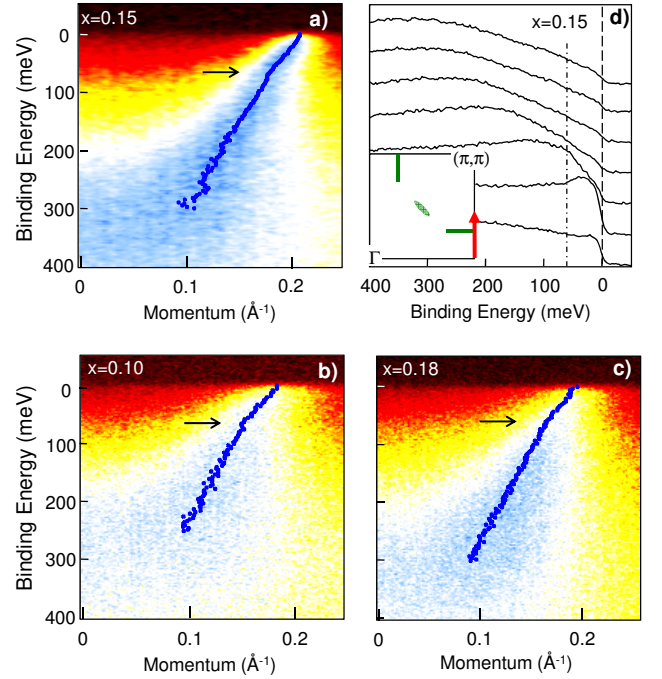


FIG. 2: (Color online) Intensity maps of ARPES data along the anti-nodal direction from (a) $x=0.15$, (b) 0.10 and (c) 0.18 samples of SCCO. As in Fig. 1, the lines are MDC dispersions and the arrows mark the energy where kinks in the dispersion exist. (d) EDC stacks of the $x=0.15$ data in (a). The vertical dash-dot line marks the kink energy.

the experimental EDCs in Fig. 1 (b) and (d), one can also see that the peaks quickly broaden beyond the energies marked by the vertical dash-dot line. Such behavior already suggests the existence of EBC in these materials.

The kink feature is not only observed along the nodal direction but also in the anti-nodal direction. Fig. 2 shows ARPES data along the $(\pi, 0)$ to (π, π) direction. The data show clear Fermi edges unlike the spectra from the nodal direction. This is because the near E_f features are from momentum points that are far enough from the anti-ferromagnetic Brillouin zone (BZ) boundary and thus the folding effect is minimal. The MDC dispersions again show kinks at the arrow-marked energy positions. With minimal folding effects in the region, one can attribute the kinks to the EBC. EDCs of $x=0.15$ Fig. 2 (d) also show that sharp peaks at the low binding energy quickly become broad beyond a certain energy, which is a clear sign of EBC. It is noted that the characteristic energy where the kink exists is at around 70 meV (compared to 50 meV for the nodal direction) and is more or less doping independent.

A natural and important question is whether such kink-like feature is an intrinsic property of electron doped HTSCs or is specific to SCCO. In that regards, investigation of other electron doped compounds is important. Shown in Fig. 3 are the data from optimally doped ($x=0.15$) NCCO and ECCO. The NCCO nodal cut in Fig. 3a shows a dispersion that crosses the Fermi en-

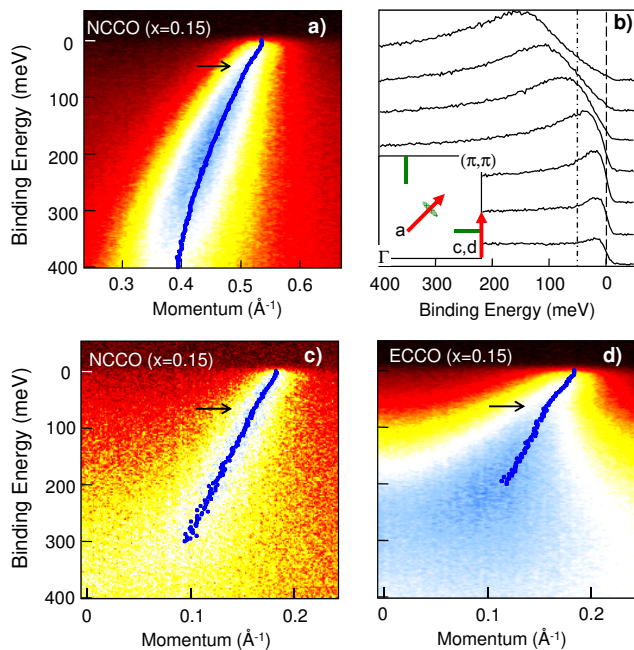


FIG. 3: (Color online) Intensity maps of ARPES data. (a) Nodal cut for NCCO ($x=0.15$) and (b) EDCs. Anti-nodal cuts for (c) NCCO and (d) ECCO ($x=0.15$).

ergy, unlike the SCCO with $x=0.15$ case. The EDCs of the data presented in panel (b) again show sudden broadening beyond a characteristic energy. On the other hand, ECCO nodal dispersion has a gap of $\approx 40\text{meV}$ and spectral features are broad. Therefore, for the same reason as the $x=0.10$ SCCO case, ECCO nodal data is not presented. This trend of the nodal gap increase when Nd is replaced by Sm and Eu is consistent with earlier observation¹⁶. For anti-nodal cuts, depicted in Fig. 3 (c) and (d), the dispersive features cross the Fermi level and show clear kink-like features near 70 meV as was the case for SCCO. The above results tell us that EBC is present in all the electron doped HTSCs, independent of the rare earth element.

For a quantitative analysis on EBC, it is useful to look at the self energies of the spectral functions. Conventionally, the real part of self energy is obtained by subtracting the bare band dispersion from the MDC dispersion and imaginary by multiplying the MDC width with the Fermi velocity. This method, however, is not applicable to the data from these materials, especially for the nodal data, because the bare band dispersion is not known due to a folding effect^{14,20}. One could think about fitting the EDCs, but it is too unreliable due to the highly asymmetric lineshape.

In such cases, one may use a newly developed method for determining the electron *removal* self energy²¹. ARPES intensity $I(k,\omega)$ is proportional to the imaginary part of electron removal Green's function or the spectral function $A(k,\omega)$. One could recover the full Green's function if one knew $A(k,\omega)$ over the entire energy range

because the real and imaginary parts of the Green's function are related through the Hilbert transform. However, this is not possible because ARPES measures the spectral function only below the Fermi energy ($\omega=0$). In that case, one can define electron *removal* Green's function which bares information on the electron dynamics only below $\omega=0$. The rest comes naturally and one can obtain the imaginary part of the electron removal self energy $\text{Im}\Sigma^R$ without any *a priori* assumptions. $\text{Im}\Sigma^R$ is then a simple algebraic expression of the ARPES spectral function and its Hilbert transform²¹. The advantage of the method is that it can be applied to any line shape and represents the “peak width” of a spectral function. For the purpose of the discussions given here, $\text{Im}\Sigma^R$ can be regarded as $\text{Im}\Sigma^{21}$.

Fig. 4a shows $\text{Im}\Sigma$ of the nodal cuts in Figs. 1 and 3. The data in panel (a) show a considerable slope change around 50 meV (vertical dashed line). For the data along the anti-nodal direction in panel (b), the slope change occurs around an increased energy of 70 meV. While the 70 meV kink observed near the anti-nodal direction has been observed in earlier studies on NCCO²², the kink at 50 meV along the nodal direction in electron doped HTSC is seen for the first time²³. The slope change around 20 meV is an artifact due to the finite energy resolution.

Our data show that there is EBC for both nodal and anti-nodal directions, at ≈ 50 and ≈ 70 meV, respectively. These mode energies are roughly independent of doping and rare earth atoms. Then the question is which bosonic mode causes the observed kink structures. Recently, it was found through neutron experiments that the energy of the spin resonance mode in electron doped HTSCs is at most 10 meV^{12,13}. Therefore, the spin resonance mode can not explain the kinks at 50 and 70 meV in the ARPES spectra from electron doped HTSCs.

Instead, it can be naturally attributed to the bond stretching mode of the copper oxygen plane. Fig. 4(c) shows the published phonon dispersions of bond stretching modes in electron doped HTSCs²⁴. We note that the energy range of the phonon dispersion is similar to that of the kink energy. It is known that electron coupling to bond stretching phonons is stronger near the BZ zone boundaries. Phase space argument can be used to show that an anti-nodal photo-hole couples to full breathing phonons ($q=[0.5,0.5,0]$, 60 meV)²⁵ and experimental results show that a nodal photo-hole mostly couples to half breathing mode ($q=[0.5,0,0]$, 50 meV)^{5,26}. This is very much compatible with the observed energy scales.

As it is clear from the above discussion that the kinks in our data are from the EPC, we try to estimate the EPC constant. Conventionally, the EPC constant λ is obtained from the mass re-normalization factor, that is, the ratio between the Fermi velocities of the bare and experimental dispersions ($\lambda = v_F^{\text{bare}}/v_F^{\text{exp}} - 1$). However, this method does not work when the band dispersion is non-linear, which is the case for SCCO. On the other hand, one can estimate λ from the $\text{Im}\Sigma$ in a more general way. The step height is already a rough measure

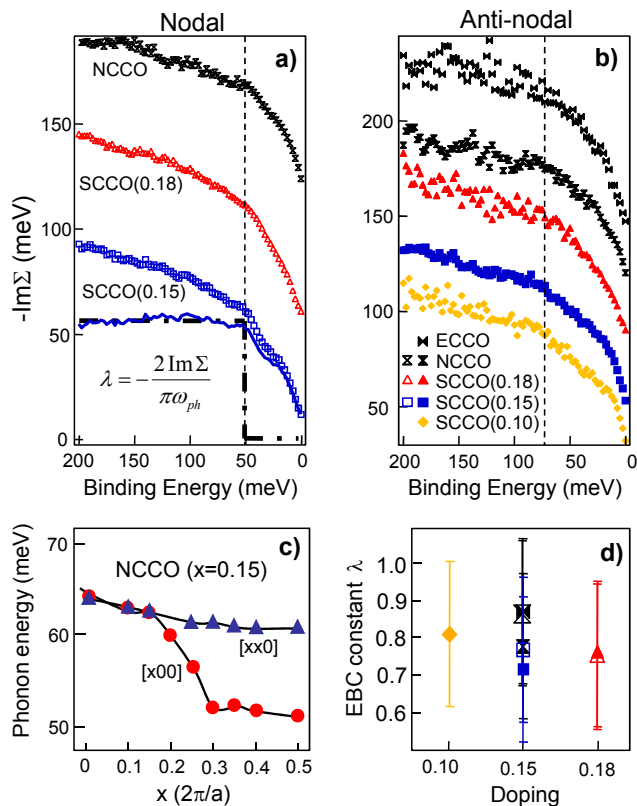


FIG. 4: (Color online) (a) Imaginary parts of self energies $\text{Im}\Sigma$ of the nodal data in Fig. 1. Curves are offset by 50 meV for clarity. The bottom curves show phonon contribution to $\text{Im}\Sigma$ after a linear background has been subtracted (solid) and theoretical $\text{Im}\Sigma$ with an Einstein phonon (dash-dot). (b) $\text{Im}\Sigma$ for the anti-nodal direction with 30 meV offset. (c) Experimental phonon dispersions of the bond stretching modes in NCCO. (d) Estimated EPC constants from $\text{Im}\Sigma$ in panels (a) and (b).

of EPC strength. To obtain the step height, one has to subtract the electron-electron interaction contribution to $\text{Im}\Sigma$. For the energy window in Fig. 4a, $\text{Im}\Sigma$ has an approximate linear background above the kink energy. The solid blue curve is the resulting $\text{Im}\Sigma$ after the linear background has been subtracted. The resulting $\text{Im}\Sigma$ is compared with an ideal $\text{Im}\Sigma$ from a single Einstein phonon at the kink energy (dash-dot line). Even though the two are different as there are multiple phonon modes, we use the single Einstein model for a rough estimate of EPC constant. In that case, the EBC constant is obtained by a simple equation given in Fig 4a. The results are plotted in Fig. 4d. Overall, the value is about $\lambda=0.8$

for both nodal and anti-nodal directions and does not vary much due to doping and rare earth atom substitution. Even though the error bars are as large as 40%, this clearly casts a sharp contrast with the hole doped cases where EBC constant in the anti-nodal region is as large as ten times that of the nodal region⁴. We can therefore say that EPC in electron doped cuprates is (relatively) isotropic.

The fact that EPC universally exists in electron doped cuprates and is similar independent of doping and rare earth elements while the T_c varies from 25 to 0 K suggests that the observed EPC in the present work may not play the dominant role in determining the superconductivity. This fact in turn implies that there must be other important factors in the superconductivity. The clue to this question could be found in comparing the present results with that of hole doped materials for which T_c 's are much higher. First of all, contrary to the electron doped materials, the EBC λ is strongly anisotropic for hole doped cuprates. Such anisotropy comes from the fact that a bosonic mode at 40 meV, either B_{1g} phonon^{5,25} or magnetic resonance mode³, preferentially couples to the electrons in the anti-nodal region. Electron coupling to this bosonic mode is much stronger than the coupling to the bond stretching phonon mode^{4,25}, and gives strong anisotropic EBC in hole doped HTSCs⁴. Secondly, the strong EBC in the anti-nodal region of hole doped HTSCs is observed only below T_c ³ while the kink structure still exists even in the normal state of electron doped HTSCs as can be seen in ECCO. Temperature dependence studies on NCCO also show no change in the kink structure across the T_c ²³.

These observations point to the fact that there is a missing bosonic mode in electron doped HTSCs that couples to the electrons in the anti-nodal region and causes strong anisotropy in hole doped materials. This disparity between the two systems may be related to the fact that the energy position of the van Hove singularity is at about 350 meV for electron doped while it is very close to the Fermi energy for hole doped materials. Independent of the origin, the missing mode could be closely related to the disparity in T_c s between electron- and hole-doped HTSCs.

We thank T. P. Devereaux, N. P. Armitage and T. Tohyama for helpful discussions. Experimental supports from D. H. Lu and R. G. Moore are acknowledged. This work is supported by the KICOS in K2060200008 and by KOSEF (R01-2006-000-10904-0). SRP acknowledges support through the BK21 Project and Seoul Science Fellowship. SSRL is operated by the DOE's Office of BES.

* Electronic address: cykim@phya.yonsei.ac.kr

¹ G. Grimvall, *The Electron-Phonon Interaction in Metals* (North-Holland, New York, 1981).

² A. Lanzara, *et al.*, *Nature* **412**, 510 (2001).

³ P. D. Johnson *et al.*, *Phys. Rev. Lett.* **87**, 177007 (2001).

⁴ A. Kaminski *et al.*, *Phys. Rev. Lett.* **86**, 1070 (2001).

⁵ T. Cuk *et al.*, *Phys. Rev. Lett.* **93**, 117003 (2004).

⁶ X. J. Zhou *et al.*, *Phys. Rev. Lett.* **95**, 117001 (2005).

- ⁷ A. A. Kordyuk *et al.*, Phys. Rev. Lett. **97**, 017002 (2006).
- ⁸ D. Reznik, B. Keimer, F. Dogan, I. A. Aksay, Phys. Rev. Lett. **75**, 2396 (1995).
- ⁹ R. J. McQueeney *et al.*, Phys. Rev. Lett. **82**, 628 (1999).
- ¹⁰ H. F. Fong *et al.*, Nature **398**, 588 (1999).
- ¹¹ P. Dai *et al.*, Science **284**, 1344 (1999).
- ¹² S. D. Wilson *et al.*, Nature **442**, 59 (2006).
- ¹³ J. Zhao *et al.*, Phys. Rev. Lett. **99**, 017001 (2007).
- ¹⁴ S. R. Park *et al.*, Phys. Rev. B. **75**, 060501(R) (2007).
- ¹⁵ F. C. Niestemski *et al.*, Nature **450**, 1058 (2007).
- ¹⁶ M. Ikeda *et al.*, J. Supercond. Nov. Mag. **20**, 563 (2007).
- ¹⁷ N. P. Armitage *et al.*, Phys. Rev. Lett. **88**, 257001 (2002).
- ¹⁸ Y. Onose, Y. Taguchi, K. Ishizaka, Y. Tokura, Phys. Rev. Lett. **87**, 217001 (2001).
- ¹⁹ S. R. Park *et al.*, J. Phys. Chem. Sol., to be published.
- ²⁰ H. Matsui *et al.*, Phys. Rev. Lett. **94**, 047005 (2005).
- ²¹ Chul Kim *et al.*, Phys. Rev. B. **76**, 104505 (2007).
- ²² N. P. Armitage *et al.*, Phys. Rev. B. **68**, 064517 (2003).
- ²³ Independent work by F. Schmidt *et al.* shows results that are consistent with ours.
- ²⁴ M. Braden, L. Pintschovius, T. Uefuji, K. Yamada, Phys. Rev. B. **72**, 184517 (2005).
- ²⁵ T. P. Devereaux, T. Cuk, Z. X. Shen, N. Nagaosa, Phys. Rev. Lett. **93**, 117004 (2004).
- ²⁶ J. Graf *et al.*, Phys. Rev. Lett. **100**, 227002 (2008).